

Simultaneous generation of quasi-monoenergetic electron and betatron X-rays from nitrogen gas via ionization injection

K. Huang,¹ D. Z. Li,² W. C. Yan,¹ M. H. Li,¹ M. Z. Tao,¹ Z. Y. Chen,³ X. L. Ge,⁴ F. Liu,⁴ Y. Ma,¹ J. R. Zhao,¹ N. M. Hafz,⁴ J. Zhang,⁴ and L. M. Chen^{1,a)}

¹Beijing National Laboratory of Condensed Matter Physics, Institute of Physics, CAS, Beijing 100190, China

²Institute of High Energy Physics, CAS, Beijing 100049, China

³Institute of Fluid Physics, China Academy of Engineering Physics, Mianyang, 612900 Sichuan, China

⁴Key Laboratory for Laser Plasmas (MOE) and Department of Physics and Astronomy, Shanghai Jiao Tong University, Shanghai 200240, China

(Received 31 August 2014; accepted 3 November 2014; published online 17 November 2014)

Upon the interaction of 60 TW Ti: sapphire laser pulses with 4 mm long supersonic nitrogen gas jet, a directional x-ray emission was generated along with the generation of stable quasi-monoenergetic electron beams having a peak energy of 130 MeV and a relative energy spread of $\sim 20\%$. The betatron x-ray emission had a small divergence of 7.5 mrad and a critical energy of 4 keV. The laser wakefield acceleration process was stimulated in a background plasma density of merely $5.4 \times 10^{17} \text{ cm}^{-3}$ utilizing ionization injection. The non-self-focusing and stable propagation of the laser pulse in the pure nitrogen gaseous plasma should be responsible for the simultaneous generation of the high-quality X-ray and electron beams. Those ultra-short and naturally-synchronized beams could be applicable to ultrafast pump-probe experiments. © 2014 AIP Publishing LLC.

[<http://dx.doi.org/10.1063/1.4902127>]

The rapid development of ultraintense femtosecond laser technology stimulates massive progress in several aspects of high energy density physics, such as laser wake field acceleration (LWFA) and ultrafast x-ray generation.¹⁻⁴ When a relativistic ($a_0 > 1$, a_0 is the laser normalized vector potential) laser pulse is incident into underdense plasma, a large amplitude electrostatic plasma wave called laser wakefield is formed behind the laser pulse. The phase velocity of the laser wakefield equals the group velocity of laser in plasma, which is close to c . Electrons trapped in a wakefield experience an accelerating field of 100GV/m, which is three orders higher than available in conventional accelerators.¹ In the nonlinear regime of LWFA, when an ultra-short ($c\tau_0 < \lambda_p$ where c is the vacuum light velocity, τ_0 is the laser pulse duration, and λ_p is the electron plasma wavelength) intense laser pulse having $a_0 > 2$,⁵ interacts with the plasma, the ionized electrons are evacuated and an ion cavity (bubble) is formed behind the laser pulse. Monoenergetic and GeV electron beams have been generated from LWFA working in bubble regime.⁶⁻¹⁰

Moreover, the accelerated electrons traveling in the plasma channel will undergo betatron oscillations due to the restoring force supplied by transverse electrostatic field in the channel. Since the electrostatic field has micrometer scale length, the electrons undergoing the betatron motion will emit x-rays along the propagation direction.¹¹ Betatron x ray sources have been achieved from laser wakefield acceleration with a source size of micrometers¹² and energies up to the γ -ray level.¹³ The wiggler strength parameter of an electron undergoing betatron movement is defined as $K = \gamma\theta$, in which γ is the Lorentz factor of a relativistic electron and θ is the x-ray beam divergence angle. When the strength parameter $K \gg 1$, the emitted x-ray has a synchrotron-like continuous spectrum

with a critical energy of $E_c = 3\hbar K\gamma^2\omega_b$, in which \hbar is the reduced Planck constant and ω_b is the betatron oscillation frequency. With the electron energy of hundreds of MeV, the generated betatron radiation can easily get into the hard x-ray region.

Most betatron x-ray sources were generated from a plasma with a density above 10^{18} cm^{-3} ,¹¹⁻¹⁵ and the electron bunches were generated from the self-injection. Since self-injection regime relies on the nonlinear wave breaking of the plasma wave, usually, the generated beams of electrons and betatron x-rays have large shot-to-shot fluctuations. Another drawback of the self-injection regime is that it usually requires a laser power much larger than the self-guiding power to get the electrons trapped in the bubble,¹⁶ thus reducing the energy transfer efficiency from laser to electrons and x-rays. Ionization injection using high Z gas is an alternative that has the advantage of lowering the injection threshold. Electron beams generated from ionization injection have been studied experimentally¹⁷⁻¹⁹ and theoretically.²⁰⁻²³ Quasi-monoenergetic electron beams have been observed from a single stage Nitrogen gas target.²⁴⁻²⁶ However, betatron x-rays emitted from ionization injection were merely studied, and the simultaneous generation of high-quality quasimonoenergetic electron and x-ray beams was scarcely observed.²⁷

In this paper, we present a simultaneous generation of quasimonoenergetic electron and betatron x-ray beams in the ionization injection regime. By interacting ultra-short laser pulses with low density pure nitrogen gas jet, no self-focusing was observed and the electrons were generated at the beginning of the process when the laser a_0 was large enough to cause ionization injection. The electron beams generated from ionization injection were highly stable and had quasimonoenergetic peaks around 130 MeV. Simultaneously, highly collimated x-ray beams with transverse divergence of 7.5 mrad were emitted in the forward direction. The x-ray spectrum had

^{a)}Electronic mail: lmchen@iphy.ac.cn

a critical energy of 4 keV by fitting with a synchrotron-type curve.

The experiment was carried out using a high power Ti:Sapphire laser system at the Key Laboratory for Laser Plasmas (LLP) at Shanghai Jiao Tong University in China. In the experiment, the system delivered laser pulses with energy up to 1.6 J and pulse duration of 30 fs at full width half maximum (FWHM). The linearly polarized laser pulses were focused by a $f/20$ off-axis parabola (OAP) onto the gas jet. The focal spot had a FWHM radius of $15\ \mu\text{m}$ with 28% of the total pulse energy contained ($1/e^2$ radius $w_0 \sim 25\ \mu\text{m}$). The resulting peak laser intensity corresponds to a normalized vector potential of $a_0 = 1.8$. The gas jet was formed from a 4 mm long supersonic nozzle. Since there is a large ionization potential gap between L-shell electrons and K-shell electrons, the charge state for the background nitrogen ions is assumed to be $5+$. The background electron density is estimated to range from $2.7 \times 10^{17}\ \text{cm}^{-3}$ to $2.7 \times 10^{18}\ \text{cm}^{-3}$ for the stagnation pressures from 0.1 bar to 1 bar. Detailed measurements on the gas density were mentioned in Refs. 28 and 29. The generated electron beams were dispersed by a 16 cm-long permanent dipole magnet with magnetic field strength of 0.98 T. The electron spectrum and x-ray signal were recorded simultaneously by setting an imaging plate (IP) (Fuji Film SR series) covered with $12\ \mu\text{m}$ aluminum foil behind the magnet. A top view imaging system was set to monitor the laser propagation in the gas target.

In the experiment, to eliminate the possibility of self-injection in the LWFA process, the laser plasma interaction was performed at very low plasma densities. At a background electron density of $5.4 \times 10^{17}\ \text{cm}^{-3}$, highly collimated and stable quasi-monoenergetic electron beams were generated. The energy spectra of three consecutive shots are shown in Fig. 1(a). The energy peaks of the spectra were $131 \pm 10\ \text{MeV}$, $128 \pm 12\ \text{MeV}$, and $134 \pm 12\ \text{MeV}$, respectively. The divergence angle of an electron beam could be deduced from the transverse profile of the recorded spectra. For the shots with quasi-monoenergetic electron beams, the transverse divergences of the beams were in the range of $3.8 \pm 0.3\ \text{mrad}$. In Fig. 1(a), we can clearly observe the long tails in shot#3. The long-tail is a common feature for electron beams generated from ionization injection which has been reported elsewhere.^{17,24} It is a result of continuous ionization and injection of the inner-shell electrons. The total charge of the electrons with energy above 50 MeV were in the range of 5.6–7.1 pC.³⁰ The deconvolved electron spectra of the three consecutive shots are plot out in Fig. 1(b).

The channel image recorded by the top view system is shown in Fig. 1(c). For 70% of the shots, when collimated electron beams were generated, the plasma channel lengths were about 2.4 mm. The laser self-focusing power threshold in underdense plasma is $P_c = 17(\omega_0^2/\omega_p^2)$ [GW], in which ω_0 is the laser frequency and ω_p is the plasma frequency. For a plasma density of $5.4 \times 10^{17}\ \text{cm}^{-3}$ and a laser wavelength of 800 nm, the critical power is 55 TW (quite high). The experiment was performed with a $P/P_c \sim 0.97$. Note that the Rayleigh length of the laser beam $Z_R = \pi w_0^2/\lambda$ is $\sim 2.45\ \text{mm}$, where λ is the laser wavelength and w_0 is the laser focal spot radius. The channel length was just about the same as Z_R . Based on the calculations, we deduced that the laser just

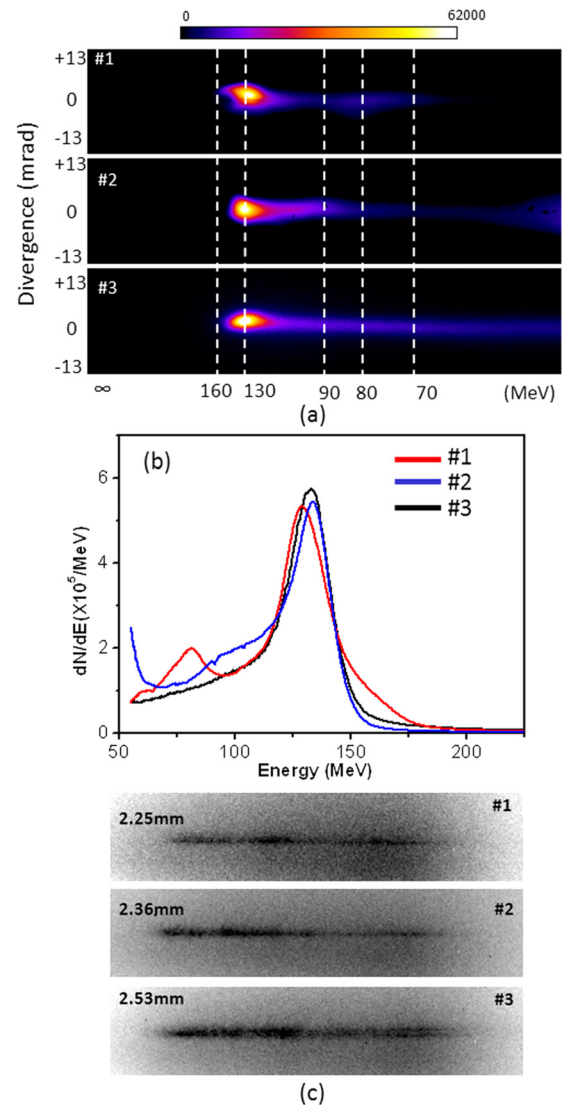


FIG. 1. Electron signal and channel image of 3 typical shots (correspondingly) (a) quasi-monoenergetic electron beam on IP for three typical shots; (b) deconvolved electron energy spectra; (c) top-view image of the plasma channel.

propagated through the gas jet and no self-focusing occurred. Without self-focusing, the laser intensity could not be enhanced further during propagation. Since the incident laser pulse had an $a_0 = 1.8$, with a plasma density of merely $5.4 \times 10^{17}\ \text{cm}^{-3}$, self-injection is impossible to take place. The ionization potentials to produce N^{6+} and N^{7+} ions are 552 eV and 667 eV, respectively. Based on previous theoretical and experimental studies,^{17,20} it is sufficient for a laser pulse with $a_0 \sim 1.8$ to ionize the N^{5+} ions to N^{6+} ions. Thus, it is reasonable to infer that the quasimonoenergetic electron beams were generated from ionization injection of the 6th electron (K-shell) located only near the peak of the laser pulse. The monoenergetic structure can be explained as follows: Since no obvious self-focusing occurred, the laser intensity kept decreasing when propagating through the gas jet. Ionization injection process would cease when a_0 falls below 1.7.²⁰ Assuming a free space propagation for a Gaussian laser pulse, the transverse spot radius is estimated to be $w^2 = w_0^2[1 + (Z/Z_R)^2]$, in which Z is the propagation distance and Z_R is the Rayleigh length. Ignoring the pump

depletion of the laser pulse, a_0 is a function of the propagation distance, which can be defined as $a = a_0/[1 + (Z/Z_R)^2]$. In our case, a dropped below 1.7 in a distance of 600 μm . So the injection process only occurred at the first 600 μm . Considering laser energy depletion by the plasma wave and in the gas ionization processes, actually that distance could be even shorter. On the other hand, the dephasing length $L_d \propto \frac{\omega_p^2}{\omega_0^2} \lambda_p$ for the electrons³¹ is calculated to be 160 mm as a result of such low plasma density. Mono-energetic structure formation due to phase space rotation is excluded since the dephasing length is much larger than the gas jet length. Thus, the short injection distance limited by the non-self-focusing propagation of the laser pulse should be responsible for the generation of quasi-monoenergetic electron beams. Since this LWFA process is working in a linear mode, the maximum acceleration gradient can be estimated by $E_0 = c m_e \omega_p / e = 70 \text{ MV/mm}$, where ω_p is the electron plasma frequency. Given a channel length of 2.4 mm, the maximum electron energy should be 170 MeV, which is in agreement with the observed spectrum in Fig. 1(b).

With stable channel formation and quasimonoenergetic electron beam generation, highly collimated x-ray beams were also generated along the laser and electrons propagation direction. Typical x-ray transverse spatial profile is shown in Fig. 2(a). The emitted x-ray beams were confined in a small divergence angle of 7.5 mrad (FWHM). With a γ of 260 ($E = 130 \text{ MeV}$), the betatron oscillation strength parameter $K = \gamma\theta$ is 2, which is relatively small compared with previous studies.^{2,12-14} The spectrum of the x-ray source was

measured by cut-off filters technique. Assuming the generated x-ray had a synchrotron-type spectrum, i.e., $S(E) \sim N_\beta \frac{3e^2}{2\pi^3 \hbar c \epsilon_0} \gamma^2 (E/E_c)^2 \cdot K_{2/3}^2(E/E_c)$, in which N_β is the number of oscillations, $K_{2/3}$ is a modified Bessel function of the second kind and E_c is the critical energy. When the photon energy $E > E_c$, the radiation decays exponentially. The filter pairs include: (1) 25 μm Al; (2) 25 μm Al + 14 μm Ti; (3) 25 μm Al + 25 μm W; and (4) 25 μm Al + 25 μm Au. The x-ray transmission after each filter is $T^i(E)$. The image plate response is $\eta(E)$.³² The calculated signal intensity after filter $I_{cal}^i(E_c) = \int S(E, E_c) T^i(E) \eta(E) dE$ should be proportional to the experimental data I_{exp}^i . By performing least squares fitting between array I_{cal}^i and I_{exp}^i , we get a best fit for an x-ray critical energy of 4 keV. The adopted x-ray fitting method is similar to that in Ref. 33. By integration of the PSL (photo-stimulated luminescence) signal on IP, the total x-ray photon number in the FWHM of the spatial beam profile is 1.6×10^7 .

Since the x-ray critical energy, betatron strength parameter, and electron energy have been measured, based on the definition of critical energy for the emitted betatron x-ray $E_c = 3\hbar K \gamma^2 \omega_b$, the oscillation frequency of the betatron oscillations is calculated to be $\omega_b = 1.6 \times 10^{13} \text{ rad/s}$. The oscillation period can be deduced as $\lambda_b = \frac{2\pi c}{\omega_b} = 100 \mu\text{m}$. Considering a channel length $L = 2.5 \text{ mm}$, the number of the betatron oscillation periods is $N_0 = \frac{L}{\lambda_b} = 25$. With a measured $K = 2$, the total photon number can be estimated as $N_x = 5.6 \times 10^{-3} N_e N_0 K = 1.2 \times 10^7$,² in which N_e is the electron number. That is in reasonable agreement with the experimental measured value. The oscillation amplitude r_0 of the electrons performing the betatron motion is 0.1 μm deduced from $K = \gamma\theta = 2\pi\gamma r_0/\lambda_b$, which is smaller compared with previous experimental results^{2,12-14} and suggests a smaller x-ray source size. Based on the results presented here, it is anticipated that utilizing PW-class laser with a large focal spot (thus a longer Rayleigh length) propagating in low density nitrogen gas, it might be possible to simultaneously generate high-energy quasimonoenergetic electron beams and highly collimated x-ray source with good spatial coherence working in a small K-parameter regime.

In conclusion, we have experimentally demonstrated a simultaneous generation of quasimonoenergetic electron beams and betatron x-rays from laser-driven low density nitrogen gas jet target via the ionization injection mechanism. Upon the interaction of 60 TW laser pulses with 4 mm long supersonic nitrogen gas jet, a directional x-ray emission was generated along with the generation of stable quasimonoenergetic electron beams having a peak energy of 130 MeV and a relative energy spread of $\sim 20\%$. The betatron x-ray emission had a small divergence of 7.5 mrad and a critical energy of 4 keV. The laser wakefield acceleration process was stimulated in a background plasma density of merely $5.4 \times 10^{17} \text{ cm}^{-3}$ utilizing ionization injection. The non-self-focusing and stable propagation of the laser pulse in the pure nitrogen gaseous plasma should be responsible for the simultaneous generation of X-ray and electron beams. Those ultra-short and naturally-synchronized beams could be applicable to ultrafast pump-probe experiments.

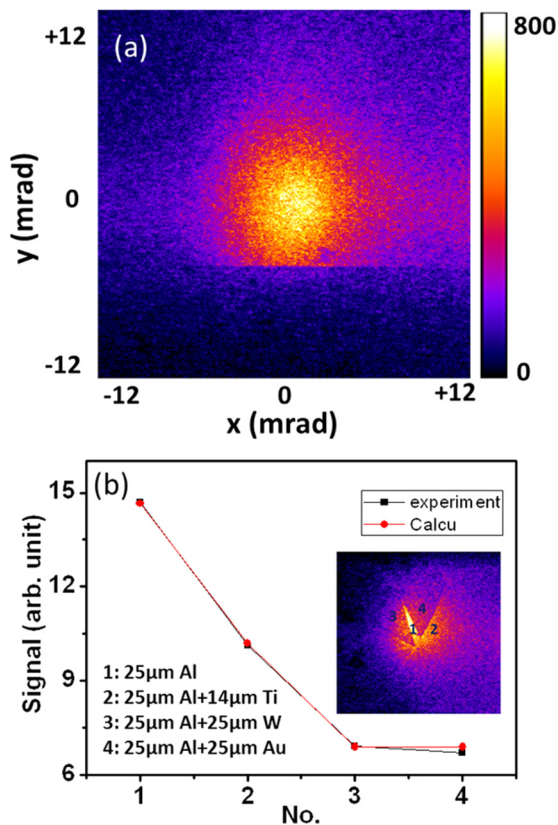


FIG. 2. X-ray measurement. (a) Typical x-ray signal on IP; (b) x-ray signal fitting using filter technology—red circles are the calculated signal using a synchrotron type curve with $E_c = 4 \text{ keV}$, and black squares are the relative experimental signal strength. The inset in (b) shows the x-ray signal after the filters. Different filter combinations are listed in (b).

This work was supported by the National Basic Research Program of China Grant No. 2013CBA01501, National Key

Scientific Instrument and Equipment Development Project No. 2012YQ120047, National Natural Science Foundation of China Grant Nos. 11334013 and 11121504, and the CAS key program.

- ¹T. Tajima and J. M. Dawson, *Phys. Rev. Lett.* **43**, 267 (1979).
- ²A. Rousse, K. T. Phuoc, R. Shah, A. Pukhov, E. Lefebvre, V. Malka, S. Kiselev, F. Burgy, J. P. Rousseau, D. Umstadter, and D. Hulin, *Phys. Rev. Lett.* **93**, 135005 (2004).
- ³N. D. Powers, I. Ghebregziabher, G. Golovin, C. Liu, S. Chen, S. Banerjee, J. Zhang, and D. P. Umstadter, *Nature Photonics*, **8**, 28 (2014).
- ⁴L. M. Chen, F. Liu, W. M. Wang, M. Kando, J. Y. Mao, L. Zhang, J. L. Ma, Y. T. Li, S. V. Bulanov, T. Tajima, Y. Kato, Z. M. Sheng, Z. Y. Wei, and J. Zhang, *Phys. Rev. Lett.* **104**, 215004 (2010).
- ⁵W. Lu, M. Tzoufras, C. Joshi, F. S. Tsung, W. B. Mori, J. Vieira, R. A. Fonseca, and L. O. Silva, *Phys. Rev. Spec. Top.—Accel. Beams* **10**, 061301 (2007).
- ⁶S. P. D. Mangles, C. D. Murphy, Z. Najmudin, A. G. R. Thomas, J. L. Collier, A. E. Dangor, E. J. Divall, P. S. Foster, J. G. Gallacher, C. J. Hooker, D. A. Jaroszynski, A. J. Langley, W. B. Mori, P. A. Norreys, F. S. Tsung, R. Viskup, B. R. Walton, and K. Krushelnick, *Nature (London)* **431**, 535 (2004).
- ⁷C. G. R. Geddes, Cs. Toth, J. van Tilborg, E. Esarey, C. B. Schroeder, D. Bruhwiler, C. Nieter, J. Cary, and W. P. Leemans, *Nature (London)* **431**, 538 (2004).
- ⁸J. Faure, Y. Glinec, A. Pukhov, S. Kiselev, S. Gordienko, E. Lefebvre, J.-P. Rousseau, F. Burgy, and V. Malka, *Nature (London)* **431**, 541 (2004).
- ⁹N. M. Hafz, T. M. Jeong, I. Choi, S. K. Lee, K. H. Pae, V. V. Kulagin, J. H. Sung, T. J. Yu, K. Hong, T. Hosokai, J. R. Cary, D. K. Ko, and J. M. Lee, *Nat. Photonics* **2**, 571 (2008).
- ¹⁰W. P. Leemans, B. Nagler, A. J. Gonsalves, Cs. Tóth, K. Nakamura, C. G. R. Geddes, E. Esarey, C. B. Schroeder, and S. M. Hooker, *Nat. Phys.* **2**, 696 (2006).
- ¹¹E. Esarey, B. A. Shadwick, P. Catravas, and W. P. Leemans, *Phys. Rev. E* **65**, 056505 (2002).
- ¹²S. Kneip, C. McGuffey, J. L. Martins, S. F. Martins, C. Bellei, V. Chvykov, F. Dollar, R. Fonseca, C. Huntington, G. Kalintchenko, A. Maksimchuk, S. P. D. Mangles, T. Matsuoka, S. R. Nagel, C. A. J. Palmer, J. Schreiber, K. Ta Phuoc, A. G. R. Thomas, V. Yanovsky, L. O. Silva, K. Krushelnick, and Z. Najmudin, *Nat. Phys.* **6**, 980–983 (2010).
- ¹³S. Cipiccia, M. R. Islam, B. Ersfeld, R. P. Shanks, E. Brunetti, G. Vieux, X. Yang, R. C. Issac, S. M. Wiggins, G. H. Welsh, M. P. Anania, D. Maneuski, R. Montgomery, G. Smith, M. Hoek, D. J. Hamilton, N. R. C. Lemos, D. Symes, P. P. Rajeev, Val O. Shea, J. M. Dias, and D. A. Jaroszynski, *Nat. Phys.* **7**, 867 (2011).
- ¹⁴F. Albert, R. Shah, K. Ta Phuoc, R. Fitour, F. Burgy, J. P. Rousseau, A. Tafzi, D. Douillet, T. Lefrou, and A. Rousse, *Phys. Rev. E* **77**, 056402 (2008).
- ¹⁵J. Ju, K. Svensson, H. Ferrari, A. Döpp, G. Genoud, F. Wojda, M. Burza, A. Persson, O. Lundh, C.-G. Wahlström, and B. Cros, *Phys. Plasmas*, **20**, 083106 (2013).
- ¹⁶D. H. Froula, C. E. Clayton, T. Doppner, K. A. Marsh, C. P. J. Barty, L. Divol, R. A. Fonseca, S. H. Glenzer, C. Joshi, W. Lu, S. F. Martins, P. Michel, W. B. Mori, J. P. Palastro, B. B. Pollock, A. Pak, J. E. Ralph, J. S. Ross, C. W. Siders, L. O. Silva, and T. Wang, *Phys. Rev. Lett.* **103**, 215006 (2009).
- ¹⁷A. Pak, K. A. Marsh, S. F. Martins, W. Lu, W. B. Mori, and C. Joshi, *Phys. Rev. Lett.* **104**, 025003 (2010).
- ¹⁸C. McGuffey, A. G. R. Thomas, W. Schumaker, T. Matsuoka, V. Chvykov, F. J. Dollar, G. Kalintchenko, V. Yanovsky, A. Maksimchuk, and K. Krushelnick, *Phys. Rev. Lett.* **104**, 025004 (2010).
- ¹⁹C. E. Clayton, J. E. Ralph, F. Albert, R. A. Fonseca, S. H. Glenzer, C. Joshi, W. Lu, K. A. Marsh, S. F. Martins, W. B. Mori, A. Pak, F. S. Tsung, B. B. Pollock, J. S. Ross, L. O. Silva, and D. H. Froula, *Phys. Rev. Lett.* **105**, 105003 (2010).
- ²⁰M. Chen, E. Esarey, C. B. Schroeder, C. G. R. Geddes, and W. P. Leemans, *Phys. Plasmas* **19**, 033101 (2012).
- ²¹C. Kamperidis, V. Dimitriou, S. P. D. Mangles, A. E. Dangor, and Z. Najmudin, *Plasma Phys. Controlled Fusion* **56**, 084007 (2014).
- ²²F. Li, J. F. Hua, X. L. Xu, C. J. Zhang, L. X. Yan, Y. C. Du, W. H. Huang, H. B. Chen, C. X. Tang, W. Lu, C. Joshi, W. B. Mori, and Y. Q. Gu, *Phys. Rev. Lett.* **111**, 015003 (2013).
- ²³M. Zeng, M. Chen, Z. M. Sheng, W. B. Mori, and J. Zhang, *Phys. Plasmas*, **21**, 030701 (2014).
- ²⁴M. Z. Mo, A. Ali, S. Fourmaux, P. Lassonde, J. C. Kieffer, and R. Fedosejevs, *Appl. Phys. Lett.* **100**, 074101 (2012).
- ²⁵A. J. Goers, S. J. Yoon, J. A. Elle, G. A. Hine, and H. M. Milchberg, *Appl. Phys. Lett.* **104**, 214105 (2014).
- ²⁶M. Z. Tao, N. A. M. Hafz, S. Li, M. Mirzaie, A. M. M. Elsied, X. L. Ge, F. Liu, T. Sokollik, L. M. Chen, Z. M. Sheng, and J. Zhang, *Phys. Plasmas*, **21**, 073102 (2014).
- ²⁷F. Albert, B. B. Pollock, J. Shaw, K. A. Marsh, Y. H. Chen, D. Alessi, J. E. Ralph, P. A. Michel, A. Pak, C. E. Clayton, S. H. Glenzer, and C. Joshi, *Proc. SPIE* **8779**, 87791Q (2013).
- ²⁸N. M. Hafz, I. W. Choi, J. H. Sung, H. T. Kim, K.-H. Hong, T. M. Jeong, T. J. Yu, V. Kulagin, H. Suk, Y.-C. Noh, D.-K. Ko, and J. Lee, *Appl. Phys. Lett.* **90**, 151501 (2007).
- ²⁹W. C. Yan, L. M. Chen, D. Z. Li, L. Zhang, N. A. M. Hafz, J. Dunn, Y. Ma, K. Huang, L. Su, M. Chen, Z. M. Sheng, and J. Zhang, *Proc. Natl. Acad. Sci. USA* **111**, 5825 (2014).
- ³⁰K. Tanaka, T. Yabuuchi, T. Sato, R. Kodama, Y. Kitagawa, T. Takahashi, T. Ikeda, Y. Honda, and S. Okuda, *Rev. Sci. Instrum.* **76**, 013507 (2005).
- ³¹E. Esarey, C. B. Schroeder, and W. P. Leemans, *Rev. Mod. Phys.* **81**, 1229 (2009).
- ³²J. Y. Mao, L. M. Chen, L. T. Hudson, J. F. Seely, L. Zhang, Y. Q. Sun, X. X. Lin, and J. Zhang, *Rev. Sci. Instrum.* **83**, 043104 (2012).
- ³³S. Kneip, S. R. Nagel, C. Bellei, N. Bourgeois, A. E. Dangor, A. Gopal, R. Heathcote, S. P. D. Mangles, J. R. Marque's, A. Maksimchuk, P. M. Nilson, K. Ta Phuoc, S. Reed, M. Tzoufras, F. S. Tsung, L. Willingale, W. B. Mori, A. Rousse, K. Krushelnick, and Z. Najmudin, *Phys. Rev. Lett.* **100**, 105006 (2008).